

# Compensation of Multiple Access Interference Effects in CDMA-based Acoustic Positioning Systems

Fernando Seco, José Carlos Prieto, Antonio Ramón Jiménez and Jorge Guevara

**Abstract**—Recently developed acoustic positioning systems operate in a CDMA (Code Division Multiple Access) configuration, in which the ranging signals between nodes are digitally modulated orthogonal codes with the same carrier frequency and overlapping in time. CDMA permits higher position update rate than the alternative TDMA (Time Division Multiple Access), but suffers from Multiple Access Interference (MAI) effects, leading to outliers in the estimated ranges, and potentially large errors in position estimation. In this communication we present and demonstrate experimentally a subtractive Parallel Interference Cancellation (PIC) method which achieves a high degree of resistance to MAI effects, and also permits us to compensate the Intersymbol Interference (ISI) caused by the limited frequency range of acoustic transducers. When evaluated empirically in an acoustic positioning system, the PIC algorithm obtains nearly total outlier cancellation for 4 operating beacons, and 2/3 reduction of outliers for a 7 beacon setup with 32 bits long codes. Outliers are further reduced (down to 2%) by the modified PIC algorithm with ISI compensation. The method outperforms alternative outlier reduction techniques like doubling or quadrupling the signal length, or using power control to adjust the relative amplitudes of the beacon signals, and permits that the system is available for positioning over 95% of the time.

**Index Terms**—Acoustic positioning systems, CDMA acoustic signals, multiple access interference mitigation

## I. INTRODUCTION

ACOUSTIC positioning systems are based on the measurement of the propagation time of acoustic or ultrasonic signals transmitted from a static network of nodes to a mobile node (or viceversa). Depending on the system's synchronicity, the measured ranges are combined with spherical or hyperbolic multilateration techniques in order to estimate the three-dimensional position of the mobile node.

Acoustic positioning's niche lies in applications where GPS is not available, and fine-grained accuracy (in the order of 1 cm) is required: personal localization indoors [1], [2], positioning of walking robots [3], autonomous vehicles [4], flying robots [5], positioning of archaeological findings [6], measuring and tracking head movement [7], [8], and other applications. General purpose ultrasonic positioning systems are also commercially available [9], [10].

Early acoustic positioning systems used low bandwidth transducers, measuring the signal's arrival time by simple

thresholding [4], [11]. These systems avoid overlap of the beacons' signals by assigning to them consecutive time slots for their transmissions [time division multiple access (TDMA)]. In this scheme, the position estimation rate is limited by the time required by all active beacons to complete an emission cycle. Improvements of acoustic and ultrasonic sensor technology and higher processor capabilities, now permit the use of Code Division Multiple Access (CDMA) techniques, in which the signals from all nodes are transmitted simultaneously, sharing a common frequency bandwidth [12], [13]. Each node is assigned a unique orthogonal digital modulated code, which permits to determine individual Times-of-Flight (TOFs) by using signal correlation at the receiver. This technique is used in the GPS system, as well as in all modern RF communication systems.

A CDMA setup permits higher position computation rate than its TDMA counterpart, but, due to the signal overlaps in time and frequency, suffers from Multiple Access Interference (MAI) effects, which result in incorrectly estimated TOFs (outliers) and large positioning errors. The use of longer orthogonal codes for the emitting beacons provides higher processing gain and more resistance to interference. However, in acoustic systems this might not be convenient since: (a) the possibility of self-interference due to multi-path propagation increases; (b) it puts higher demands on processor memory and computation power; (c) in outdoor environments, the coherence of long signals can be destroyed by non-ideal signal propagation caused by air turbulences or temperature gradients [14], which degrades signal correlation.

The goal of the present research is to show how subtractive interference cancellation algorithms currently used in CDMA wireless communications [15], are able to compensate MAI effects in acoustic positioning systems. As far as we know, only one previous paper [12] has mentioned the use of MAI compensation techniques for CDMA-based acoustic or ultrasonic systems operating in air. Thus, the novelty of our work lies in the adaptation of a subtractive technique for MAI compensation from the wireless communications to the acoustic positioning fields, including a discussion and an experimental demonstration of its performance in detail.

The paper is organized as follows: the next section introduces the technique for subtractive interference cancellation in acoustic signals proposed in this work. Section III describes the acoustic positioning system with which we will carry out the experimental work. Section IV gives quantitative results on the performance of MAI reduction and its impact on

The authors belong to the Localization and Exploration for Intelligent Systems (LOPSI) group, Center for Automation and Robotics (CSIC-UPM), Ctra. de Campo Real km 0,200, 28500 Arganda del Rey, Madrid, Spain. Corresponding e-mail: fernando.seco@csic.es

the tracking of several trajectories of a mobile node. It also offers a comparison of the proposed method with alternative techniques for interference reduction such as power control or use of longer signal codes. Finally, we offer some conclusions in section V.

## II. COMPENSATION OF MAI AND ISI EFFECTS

### A. Description of the problem

Assuming that the positioning system has  $N$  operating emitter beacons at known locations, each transmitting a digitally modulated coded signal  $g_j(t)$ ,  $j = 1, \dots, N$ , the acoustic signal received by the mobile beacon is:

$$r(t) = \sum_{j=1}^N A_j \cdot (h_j * g_j)(t - t_j) + n(t), \quad (1)$$

where  $t_j$  and  $A_j$  are respectively the time of flight and amplitude of the signal arriving from the  $j$ -th beacon, and  $n(t)$  stands for white, uncorrelated noise. The convolution operator  $*$  denotes the filtering effect produced by the acoustic channel impulse response  $h_j(t)$ , which is a priori unknown since it depends on the relative orientation of emitter and receiver.

A conventional correlator bank (which we will call the ‘simple receiver’ in this work) produces the correlation of signal  $r(t)$  with all active signal codes; the output of the  $k$ -th element of the correlator bank is:

$$R_{r g_k}(t) = A_k \cdot (h_k * R_{g_k g_k})(t - t_k) + \sum_{j \neq k} A_j \cdot (h_j * R_{g_k g_j})(t - t_j) + \eta(t), \quad (2)$$

where  $R_{g_k g_j}(t)$  is the cross-correlation of codes  $g_k(t)$  and  $g_j(t)$ , and the commutative property of the convolution and correlation operators [16] has been utilized. This result can be written compactly as:

$$R_{r g_k}(t) = A_k \cdot (h_k * R_{g_k g_k})(t - t_k) + \text{MAI}_k + \eta(t). \quad (3)$$

In 3, the first term on the right side is the autocorrelation of the emitted code with itself, distorted by the channel response  $h_j(t)$ , which causes Intersymbol Interference (ISI). The second term ( $\text{MAI}_k$ ) represents Multiple Access Interference from all the other beacons emitting simultaneously in the cell, caused by the non-perfect orthogonality of digital codes  $g_j(t)$ . The simple receiver suffers from two shortcomings: (a) it does not model the channel response of each transducer; and (b), it follows a single-user approach that treats the MAI signals from other users as noise. The added effect of both approximations degrades severely the TOF estimates in acoustic CDMA positioning systems.

Interference due to MAI and ISI effects is found in most CDMA communication systems, for example in the uplink of mobile telephony [17], and in underwater acoustic data transmission [18]. Often, interference effects are the most important limiting factor of a communication cell capacity. Techniques for interference compensation in communication systems focus in decoding correctly the transmitted digital message, and signal delays, phases and amplitudes are relatively constant parameters that are estimated at startup; in acoustic positioning

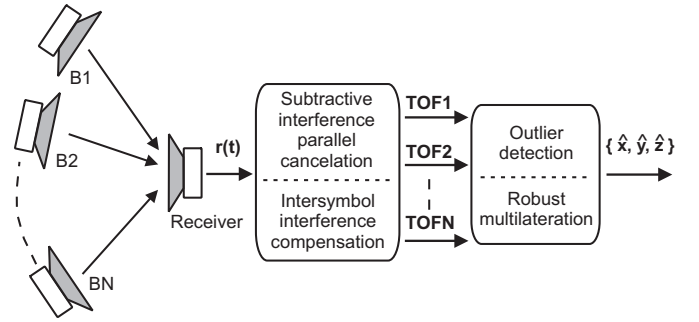


Fig. 1. Processing architecture at the receiving beacon for CDMA-based positioning with MAI compensation, consisting of the times-of-flight estimation module with interference cancellation techniques, and a robust multilateration with outlier detection module.

applications the message is not relevant, and the goal is to compute time delays with maximum accuracy.

Practical (suboptimal) algorithms for MAI cancellation are mainly divided in two categories [15]. Linear detectors apply a linear transformation to the output of the correlator bank, corresponding roughly to the inverse of the codes cross-correlations. This technique is most suited to message decoding once reasonably good estimates of delays and amplitudes of the received signals are known. In contrast, in subtractive techniques the receiver creates (re-encodes) the emitted signals with the estimated amplitudes and delays and subtracts them from the received signal in order to obtain a version free of the interfering effects of other beacons. This method works well for estimation of message or only estimation of delays and amplitudes [17], and, for its inherent simplicity, will be the approach followed in this communication.

In this work, ISI effects will be compensated by estimating the impulse response of each acoustic channel simultaneously with the MAI cancellation process. We will model the impulse response of the  $j$ -th transmitter as:

$$A_j \cdot (h_j * g_j)(t) \simeq \sum_{i=1}^{M_j} \hat{A}_{ji} g_j(t - \hat{t}'_i), \quad (4)$$

where  $M_j$  is a (variable) number of copies of the emitted code  $g_j(t)$ . The time delays  $t'_i$  are not discretized, and do not necessarily correspond to integer multiples of the sampling or symbol times. If ISI is not compensated,  $M_j = 1$ .

The details of the MAI/ISI compensation algorithm are given next.

### B. Subtractive parallel interference cancellation of MAI/ISI effects

The general design for CDMA-based acoustic positioning followed in this work is shown in Fig. 1, and the specific module which contains the subtractive parallel interference cancellation algorithm is detailed in Fig. 2. Its operation consists on the following stages:

- 1) **Initial computation of correlations.** A correlator bank produces initial estimates of the amplitudes  $\hat{A}_{k1}$  and delays  $\hat{t}_{k1}$ , by correlating  $r(t)$  with the set of emitted codes  $g_k(t)$ . These estimates are computed from the peak of

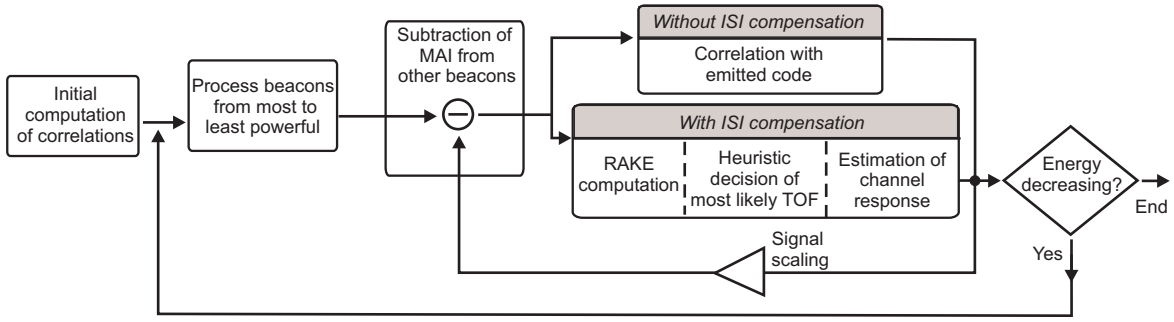


Fig. 2. Block diagram of the subtractive parallel interference cancellation module.

the correlation, which is parabolically interpolated to achieve subsample precision for the times of flight [19].

- 2) **Loop for beacon processing.** The beacons are ordered in descending initial amplitudes, so more powerful beacons will be processed first.
- 3) **Subtraction of MAI from other beacons.** For the  $k$ -th beacon, we form signal  $r_k(t)$  by subtracting the estimated components from all other beacons:

$$r_k(t) = r(t) - \sum_{\substack{j=1 \\ j \neq k}}^N \sum_{i=1}^{M_j} \hat{A}_{ji} g_j(t - \hat{t}_{ji}). \quad (5)$$

The signal  $r_k(t)$  is the receiver's current best estimate of the signal coming exclusively from the  $k$ -th beacon.

The next step of the algorithm depends on whether ISI effects will be compensated or not. If ISI is not compensated, improved estimates of  $\hat{A}_{k1}$  and  $\hat{t}_{k1}$  are produced by correlating  $r_k(t)$  with  $g_k(t)$ . However, if we desire to compensate ISI effects, the method proceeds in stages 4-7 detailed next:

- 4) For the  $k$ -th beacon, we use a **rake-like structure** [20] to produce an array of  $M'_k$  fingers (possible positions of the received code) by correlating and subtracting repeatedly  $r_k(t)$  with the emitted code  $g_k(t)$ .  $M'_k$  is an integer number such that  $M'_k \sim \hat{A}_{k1}$ ,  $M'_k \geq 1$ , and  $\sum_k M'_k = N \cdot M$ . The logic behind this is that the impulse response of the strongest signals is computed with more detail so they are canceled more thoroughly. Computation of all  $M'_k$  fingers is achieved with a single correlation operation:

$$R_k^{(1)}(t) = R_{r_k g_k}(t). \quad (6)$$

The maximum value of  $R_k^{(1)}(t)$  corresponds to the first finger, with improved amplitude  $\hat{A}_{k1}$  and time delay  $\hat{t}_{k1}$ . The positions for fingers  $i = 2, \dots, M'_k$  are found by time shifting and subtracting the known autocorrelation of the  $k$ -th code:

$$R_k^{(i)}(t) = R_{r_k g_k}(t) - \sum_{j=1}^{i-1} \hat{A}_{kj} R_{g_k g_k}(t - \hat{t}_{kj}). \quad (7)$$

This permits to avoid time-consuming correlation operations. As in step 1, no assumption is made that the TOFs coincide with sampling or symbol times.

- 5) If all  $M'_k$  computed fingers corresponded to the true signal from beacon  $k$ , we could simply choose the one with the largest positive amplitude  $\hat{A}_{ki}$  as the most likely position for the TOF. However, this produces poor results for the lowest amplitude signals, for which the most powerful finger might actually be a cross-correlation peak from an interfering beacon not perfectly eliminated by step 3 above. We need a reliable way to distinguish the set of fingers actually corresponding to the true signal from the  $k$ -th beacon from those arising from interfering beacons. The following heuristic procedure for selecting the most probable finger gives satisfactory results in our setup. For all computed fingers with positive amplitudes, the signal  $r_l(t)$  is demodulated by translating it to the baseband and sampling it at the bit intervals:

$$y_l[n] = r_l^{\text{BB}}(\hat{t}_{kl} + n \cdot T_{\text{bit}}), \quad l \in \{1, \dots, M'_k \mid \hat{A}_{kl} > 0\} \quad (8)$$

where  $T_{\text{bit}}$  is the bit period.

The most likely finger for the correct position is the one which maximizes the similarity of the demodulated signal and the code transmitted by the  $k$ -th beacon, multiplied by the amplitude of the finger itself:

$$l_{\text{opt}} = \arg \max_l \frac{|y_l[n] \cdot g_k[n]|}{|y_l[n]|} \cdot \hat{A}_{kl}. \quad (9)$$

- 6) As a result,  $\hat{t}_{kl}$  and  $\hat{A}_{kl}$  with  $l = l_{\text{opt}}$  are taken as the best estimates of the TOF and amplitude of the signal from the  $k$ -th beacon. Those fingers whose TOFs are not close enough to  $\hat{t}_{kl}$ , as given by:  $\hat{t}_{ki} - \hat{t}_{kl} > T_b$  or  $\hat{t}_{ki} - \hat{t}_{kl} < -T_a$ , are regarded as MAI terms and discarded, while the remaining  $M_k$  fingers (with  $M_k \leq M'_k$ ) are considered to belong to the impulse response of the transducer, estimated as:

$$A_k \cdot (h_k * g_k)(t) \simeq \sum_{i=1}^{M_k} \hat{A}_{ki} g_k(t - \hat{t}_{ki} + \hat{t}_{kl}). \quad (10)$$

The lower ( $-T_a$ ) and upper ( $T_b$ ) time limits of the impulse response of the transducer are fixed parameters determined experimentally.

- 7) As other researchers have noted [15], subtracting wrong amplitude and TOF estimates from the received signal might cause large errors, particularly in the first

iterations of the subtractive algorithm. For this reason, we scale the computed amplitudes by the confidence we have in the estimate of the beacon's TOF; as a confidence value we use the number of bits correctly decoded in step 5:

$$\hat{A}_{ki} = \frac{\text{correctly decoded bits}}{\text{signal bit length}} \cdot \hat{A}_{ki} \quad i = 1, \dots, M_k. \quad (11)$$

- 8) The process is repeated for all beacons and then iteratively from step 2 above. The loop finishes when the energy of the residual signal obtained by subtracting all codes and all fingers from the original signal:

$$E = \left[ r(t) - \sum_{k=1}^N \sum_{i=1}^{M_k} \hat{A}_{ki} g_k(t - \hat{t}_{ki}) \right]^2 \quad (12)$$

stops decreasing, or when the TOFs  $\{\hat{t}_{k1}\}$  differ by less than  $1 \mu\text{s}$  from those computed in the previous iteration. This guarantees quick convergence of the iterative method.

Since the interference received by every user from all other users is eliminated simultaneously, this scheme corresponds to an (iterated) Parallel Interference Cancellation (PIC) implementation [21]. In the remaining of this work, we will refer to this technique as PIC receiver, and, if additionally, intersymbol interference is compensated, as PIC/ISI receiver. Subtractive techniques are not expected to provide perfect interference cancellation, especially in the case where multipath or non line of sight propagation occurs. Although these effects can be also incorporated in the PIC algorithm, the strategy followed in the acoustic positioning system of this work is to post-process them in a robust multilateration module with outlier rejection, as shown in the final stage in Fig. 1. More information about robust positioning techniques is found in references [22] and [23].

### III. DESCRIPTION OF THE EXPERIMENTAL SYSTEM

#### A. System setup

MAI compensation techniques will be tested empirically with an acoustic local positioning system developed by our group and called 3D-Locus (see Fig. 3). This system is highly configurable [24], and has been used previously for the reliable and accurate positioning of archaeological findings, as described in [6].

The system is installed in a robotic cell, of  $2.8 \times 2.8 \times 2.8$  meters of size, with the static network of 7 emitting beacons placed in its top part and looking downwards. These beacons lie approximately on a plane, with maximum differences in height of about  $\pm 2.5$  cm. Fig. 4 shows a 2D-view of the beacon arrangement as well as two sample trajectories described later. The receiving beacon is attached, in an upward position, to the tip of a Staubli robotic arm, model RX90, which is used for controlled positioning within the cell. The quoted positioning repeatability of the arm is  $30 \mu\text{m}$ , well below the accuracy or resolution of the 3D-Locus system. The reference frame of the robot arm (whose origin is placed 1.2 m above the floor) is used for all coordinates given in this work.

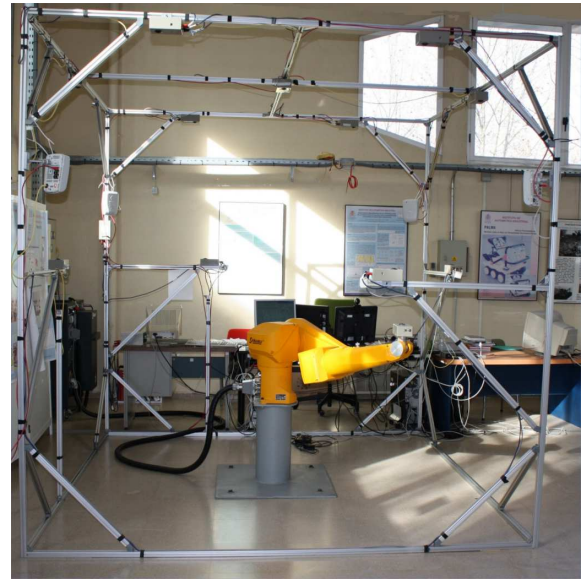


Fig. 3. The 3D-Locus acoustic positioning system: the receiving beacon is attached to the tip of the Staubli robotic arm, and the network of transmitting beacons are placed at the top of the cell's structure (looking downwards).

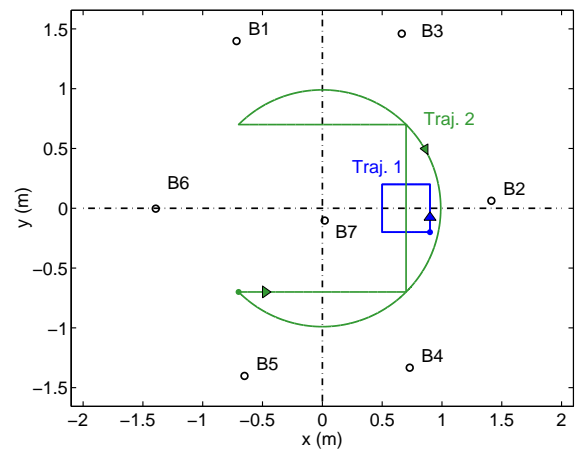


Fig. 4. The  $(x, y)$  positions of the emitting beacons (B1-B7), and the two trajectories of the robotic arm used in the experiments, as seen from a point above the robotic cell.

#### B. Spread spectrum acoustic signals

Each acoustic beacon is equipped with a Visaton CP13 tweeter speaker (emitter), and a Panasonic WM61 microphone (receiver). Their combined frequency range is 5-25 kHz, with approximately flat response (gain and phase) within that range, if emitter and receiver are placed front to front. The response, however, deteriorates if the relative angle between them increases [24].

Each beacon is programmed to transmit a binary-phase (BPSK) modulated digital signal, encoded by a single Golay code  $g_k$  with a length of 32 (the default value), 64 or 128 bits, with 1 cycle per bit, and 15 kHz carrier frequency, chosen in the central point of the system bandwidth. Golay codes are used since their correlations can be computed efficiently [25]; however, the methods in this work are generally applicable to any family of digital orthogonal codes.

The acoustic signals are received by the microphone, amplified and bandpass filtered, and sampled at 150 kHz by the processing unit present in each beacon (a TMS320F2812 microcontroller from Texas Instruments). The acquisition time is 13.7 ms (2048 points), and the dynamic range is 12 bits.

For the following experiments, the 3D-Locus system is programmed so that all nodes from the static network transmit simultaneously (CDMA). Synchronization to the receiving beacon is achieved by an electric pulse, so spherical trilateration is possible for computing the mobile node's position.

Typical SNR values of the received signal vary between 10 and 25 dB for trajectories of the mobile node below the beacon network, depending on the range and relative angle between emitter and receiver. The 3D-Locus system permits to set the signal amplitude of each emitting beacon individually, but only during startup of the system (not modifiable dynamically).

### C. Test trajectories

The receiving beacon, attached to the tip of the robotic arm, is moved in controlled trajectories under the transmitting beacon network. Two sample trajectories will be considered in this work (Fig. 4).

The first trajectory is restricted to a small area in the workspace of the robot: a horizontal square of 0.4 m of side oriented along the  $xy$  axes and centered at coordinates (0.7, 0, 0.55) m (approximately 1.1 m below the beacon network). This square is traversed twice, at a linear speed for the tip of the robot of 20 mm/s, taking approximately 175 s to complete the trajectory (the extra time is caused by the robot arm accelerating and decelerating at each vertex of the square).

The second trajectory is intended to be as wide as permitted by the reach of the robotic arm. It consists of three sides of a horizontal square, each of 1.4 m of length, and centered at the coordinates (0, 0, 0.4) m, traversed at 30 mm/s, a pause of 10 s, and then a circular trajectory that returns to the starting point along the path that covers the largest angle, at a speed of 60 mm/s. It takes about 230 s to complete this trajectory.

The emission repetition rate achieved by the 3D-Locus system during these experiments was 1.25 Hz; this is lower than the normal speed (10 Hz) since it was configured to transmit the acoustic waveforms acquired by the moving beacon to the central PC for offline processing and analysis. Thus, about 200 to 300 emissions are produced during completion of the sample trajectories 1 and 2.

The 'true' TOFs are determined from the known trajectory of the robotic arm and the position of the emitting beacons, including compensation of the effect of temperature on the speed of sound. The synchronization between 3D-Locus program and robot motion is manual.

## IV. EXPERIMENTAL RESULTS OF MAI COMPENSATION

This section describes a series of experiments performed with the 3D-Locus acoustic positioning system, aimed at demonstrating the efficacy of the MAI subtractive compensation method introduced in section II.

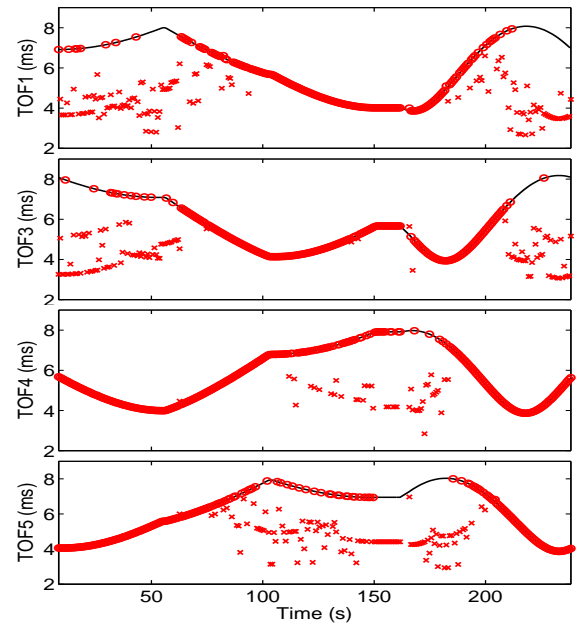


Fig. 5. TOF time sequences obtained for trajectory 2 tracked with beacons B1, B3, B4 and B5, using the conventional correlator bank without MAI compensation. The circles correspond to TOF estimated within 133  $\mu$ s of the true TOF (black continuous curve); the crosses to TOF outliers.

### A. The effect of Multiple Access and Intersymbol Interference

Consider the 3D-Locus system tracking trajectory 2 with beacons B1, B3, B4 and B5 transmitting simultaneously. Using the conventional correlator bank (simple receiver) for measurement of TOF, the time sequences shown in Fig. 5 are obtained. About 31.9% of estimated TOF are outliers largely deviated from the true values (in this work, we define an outlier as a TOF with an equivalent range error larger than two wavelengths,  $2\lambda = 45$  mm, or, equivalently, a timing error of 133  $\mu$ s). These large, non-gaussian TOF errors make those particular beacons unusable for position estimation. Referring to the trajectory shape in Fig. 4, it's seen that outliers are mostly produced when the transmitting beacon is at a larger distance, or seen from a wider angle, from the receiver, resulting in lower relative amplitude and decorrelation caused by signal distortion with angle. This is a manifestation of the 'near-far' phenomenon, in which large amplitude signals in a CDMA setup render weaker signals useless for positioning or communication. For acoustic signals, the near-far effect is further aggravated by the reduced bandwidth of acoustic transducers at off-axis angles [24].

As discussed in section II-A, limitations in the bandwidth of the acoustic channel cause intersymbol interference (ISI), and degrade positioning, even if MAI is compensated by subtractive techniques. In the 3D-Locus acoustic system, ISI effects are particularly serious when the relative angle between the emitter and receiver transducers is large, and should be controlled in order to maintain high accuracy positioning.

Fig. 6 shows the effect of ISI effect compensation, by plotting the code correlations with four beacons of the system activated, and the receiving beacon placed at an arbitrary static location. Intersymbol interference degrades signal correlation,

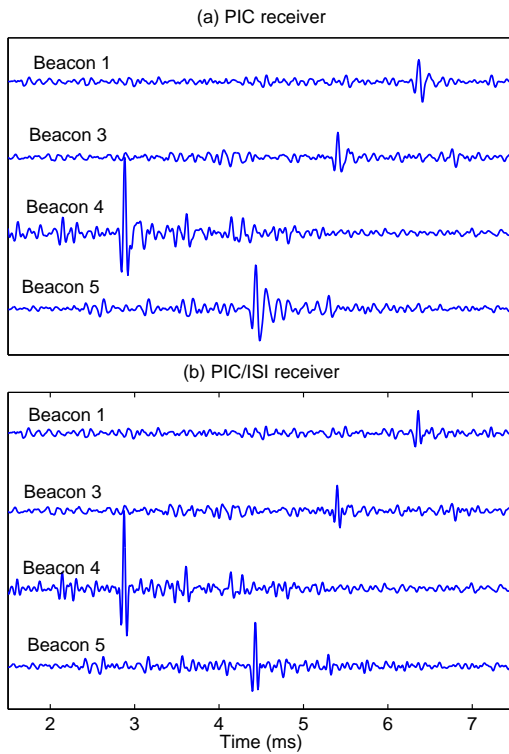


Fig. 6. Correlations of received codes, obtained by the subtractive MAI algorithm before and after compensation of ISI effects, for a setup of four emitting beacons.

and beacons with lower amplitudes are particularly vulnerable, since their signals might lie below the cross-correlation noise of closer beacons, becoming undetectable. After application of the MAI subtractive algorithm with ISI compensation, the disturbing signals are partially removed, and the correlations nearly restored to their theoretical shapes. Alternatively, the removal of ISI effects can be seen in Fig. 7, where we plot the eye patterns of the demodulated BPSK signals ( $r_l^{BB}(t)$  in (8)). Although the information conveyed by the signals is not relevant (since codes  $g_k$  are previously known), the larger aperture of the corresponding eye diagrams show that the signals can be successfully demodulated, and that decorrelation effects caused by ISI are decreased.

The impulse response of the four transmitters, as estimated by the PIC/ISI processor (10), is given in Fig. 8. Note that a variable number of fingers has been assigned to each emitter by the method. For each beacon, the finger with the largest positive amplitude corresponds to the system's estimate of the correct TOF, and the time window for the impulse response is taken as  $(-T_a, T_b) = (-2/f_0, 4/f_0) = (-133, 267) \mu\text{s}$  with respect to this TOF.

For the results shown in this section, we have used an average number of  $M = 10$  fingers/beacon in order to model each beacon's acoustic channel. However, we have checked experimentally (see section IV-F) that  $M = 5$  fingers/beacon provides almost as good reduction of the number of TOF outliers, and requires significantly less processing time. For this reason, the remaining experiments in this article involving the PIC/ISI receiver are performed with 5 fingers per beacon.

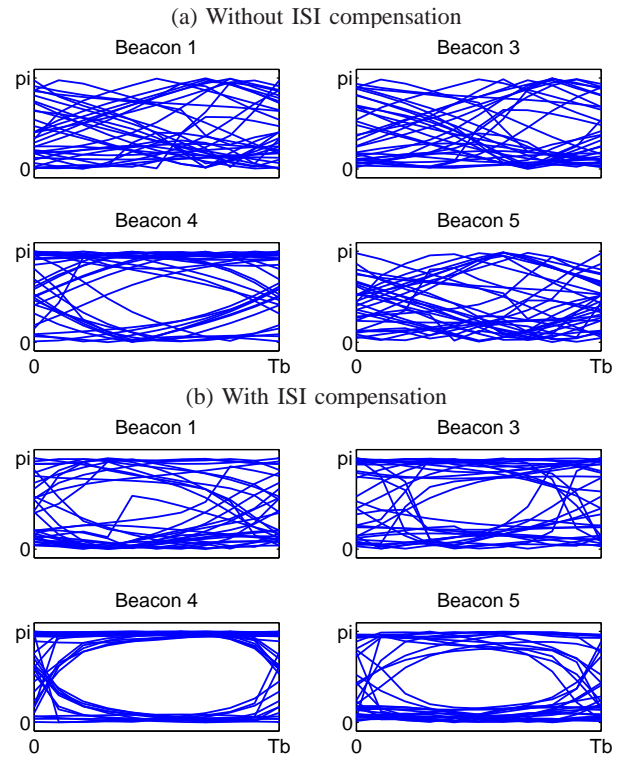


Fig. 7. The eye diagrams of the demodulated phase of the received codes, for a setup of four emitting beacons, show that the subtractive PIC/ISI algorithm is successful in eliminating most of ISI effects in the system.

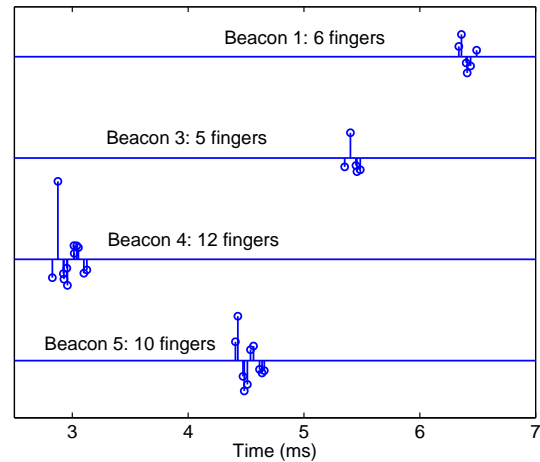


Fig. 8. Impulse response of the four transmitters, as estimated by the PIC/ISI receiver.

### B. Positioning with 4 active beacons

This section shows the performance of MAI compensation techniques when the 3D-Locus system uses 4 transmitting beacons, the minimum setup for estimation of the position of the mobile beacon, if all 4 TOFs in a given emission are estimated without outliers. In that circumstance, the position can be computed robustly by spherical multilateration, since there is enough redundancy to detect outliers. If the number of available beacons is 3, the position can be computed, but the system can not guarantee its correctness (it might be usable for tracking the displacement of the mobile node from

a previously known position).

We begin with the positioning results for trajectory 1 tracked with four beacons, in two different circumstances. In the first case we use the network formed by beacons B2, B3, B4 and B7; this is an optimal situation since the trajectory is placed right under the beacon subnetwork (refer to Fig. 4). The experimental results are shown in Fig. 9 (top). The use of the simple receiver (correlator bank) results in 16.1% of outliers in the TOF estimates; this decreases to 0.2% and 0% with the PIC and PIC/ISI algorithms, respectively. In these circumstances, the position could be estimated for 42.2, 99.1 and 100% of emissions, respectively. As we can see, this is a case of perfect compensation of MAI effects, even with the simplest version of subtractive cancellation, and a positioning system operating with the minimum number of beacons.

This very favorable situation changes if we choose four beacons placed relatively far from trajectory 1, like beacons B1, B5, B6 and B7 (the cell opposite of the one considered above). The combination of farther ranges from the emitting beacons and larger off-axis angles results in a (mean) SNR drop of -4.5 dB with respect to the well-placed beacon cell, and an increased amount of TOF outliers with the simple receiver (27.3% of emissions against 16.1% above). With the use of the PIC and PIC/ISI versions of subtractive cancellation, outliers are reduced to 0.6% and 0%, respectively, and the mobile beacon's position, which could be tracked for only 22.8% of emissions with the simple receiver, can be computed now in 97.4% and 100% of cases (Fig. 9 (mid part)). Notice how in the case of PIC cancellation without ISI compensation, some points deviate from the true trajectory, sometimes by as much as 50 mm. These points correspond to emissions where the MAI-caused errors on TOF estimates, although still below the outlier definition threshold, are amplified considerably by the bad geometric configuration of the cell (high dilution of precision). Most of these errors are eliminated by compensating ISI effects.

Similar results are obtained when tracking trajectory 2 with beacons B1, B3, B4 and B5, as seen in Fig. 9 (bottom). The simple receiver produces a total of 31.9% outliers in the TOF estimates (check the TOF traces presented in section IV-A), and the requisite that all four TOF are computed without outliers is fulfilled only for 18.3% of the signal emissions, resulting in a completely discontinuous trajectory. Notice in particular how one side of the square and the return circular path of the trajectory could not be tracked at all. After application of MAI cancellation a large reduction in the number of outliers is obtained: down to 2.2% in its simpler version, and down to 0.8% if PIC/ISI is used. In the same way, the system availability (condition that all four TOFs are correctly estimated) increases to 93.0 and 98.0% of time instances respectively), with the result that the trajectories are correctly tracked this time.

These three examples show that, when operating with a 4-beacon positioning cell and 32 bits long codes, the subtractive cancellation techniques described in section II-B almost perfectly eliminate MAI effects, even without ISI compensation (less than 2% of outliers remain). In the next section, we will consider operation of the system with all 7 beacons enabled.

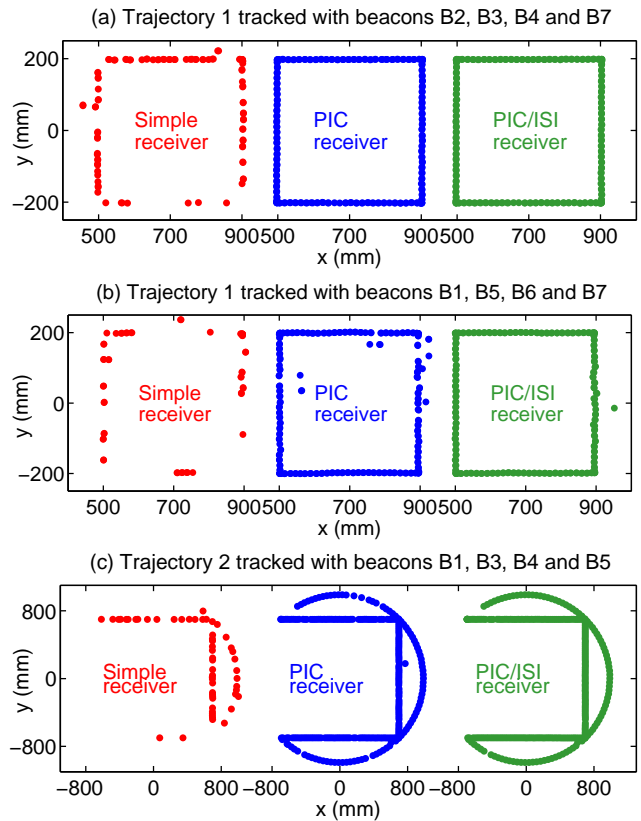


Fig. 9. Experimental results of trajectories 1 and 2 tracked with different configurations of four beacons each.

### C. Positioning with 7 active beacons

When we activate all 7 beacons of the 3D-Locus system, we expect larger MAI effects. Fig. 10 shows the results of tracking trajectories 1 and 2 with all beacons. For trajectory 1, the total percentage of outliers with the simple receiver is 46.5%, which is reduced to 16.5% and 2.2% when the PIC and PIC/ISI versions of subtractive compensation are applied. Correspondingly, the positioning capability of the system increases from the original 60.3% of emissions to 96.7% (PIC receiver) and 100% (PIC/ISI receiver), respectively. Very similar results are obtained when tracking trajectory 2 with all beacons active. Outliers are reduced from 40.0% of TOF measurements down to 9.8% (PIC) and 0.9% (PIC/ISI). The positioning system availability is increased from 81.2% (simple receiver) to 100% in both instances of MAI compensation.

In conclusion, for 7 active beacons, the simple receiver results in more than 40% of TOF outliers; this figure is reduced three times by the simple PIC method, while PIC compensation with ISI mitigation achieves almost perfect outlier compensation. Which version to implement in the positioning system depends on the beacon redundancy, the required positioning availability, and the processing capability of the receiving beacon.

### D. Positioning accuracy

In this section we study the impact on positioning accuracy of the PIC and PIC/ISI techniques. For this purpose, we have

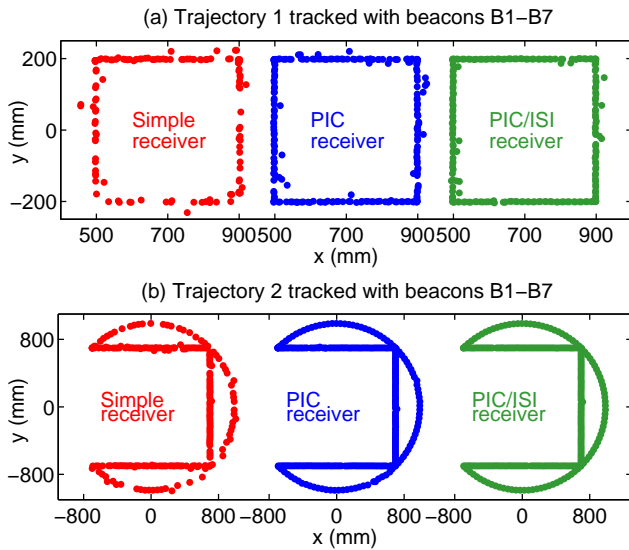


Fig. 10. Experimental results of trajectories 1 and 2 tracked with all 7 beacons of the positioning system.

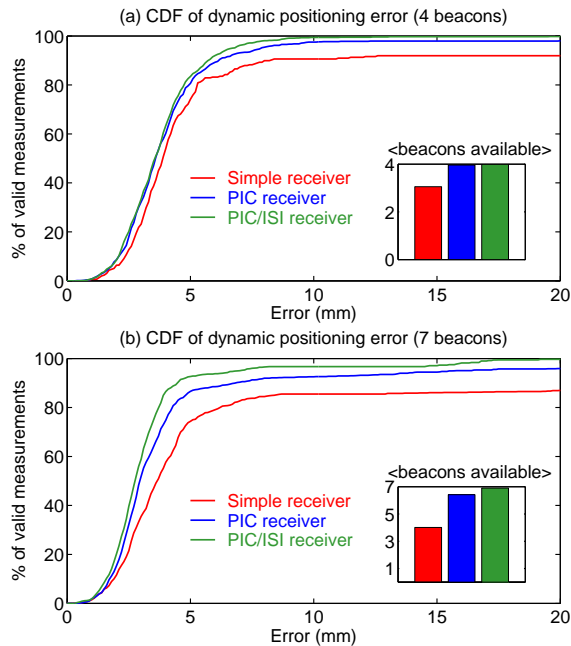


Fig. 11. CDF of dynamic positioning error obtained with the 4- and 7-beacon networks, before and after application of MAI compensation techniques. The results have been aggregated from trajectories 1 and 2. The mean number of available beacons with correct TOF estimates in each situation is shown in the inset graph.

collected all the measurements with the 4-beacon and 7-beacon networks presented above and showed them as cumulative distribution function (CDF) curves of the dynamic positioning error in Fig. 11. The numerical data from the CDF curves is also summarized in table I.

For both 4- and 7-beacon networks, the biggest impact of MAI compensation techniques lies in the increase of the number of valid TOFs per emission. With 4-beacons, an average of 3.1 (simple receiver) to almost 4 (both PIC and PIC/ISI receiver); for 7 beacons, 4.0 (simple) to 6.4 (PIC), and

TABLE I  
SUMMARY OF CDF RESULTS FOR DYNAMIC POSITIONING  
CORRESPONDING TO FIG. 11.

Emitting beacons	Receiver	Positioning error (mm)			Availab. (%)	Mean no. correct TOF
		Mean	50%	90%		
4	Simple	6.3	3.9	8.3	29.9	3.1
	PIC	4.6	3.6	6.2	96.6	3.9
	PIC/ISI	3.9	3.6	5.8	99.3	4.0
7	Simple	7.5	3.7	26.0	71.5	4.0
	PIC	4.4	3.0	6.9	98.5	6.4
	PIC/ISI	3.3	2.8	4.5	99.9	6.9

6.9 (PIC/ISI receiver). This causes a corresponding increase in the positioning availability (the condition that at least four valid TOFs are produced for a given emission). There is also an increase in positioning accuracy (mean value of positioning error), but since the 3D-Locus robust positioning stage filters out the TOF outliers before trilateration, this benefit is mostly noted in the large positioning error part of the CDF curve (check the values for the 90% errors for each method). Finally, the 7-beacon network overcomes the 4-beacon network in terms of positioning accuracy, but only if MAI compensation with ISI reduction techniques are applied.

These results compare favorably with those obtained previously with the 3D-Locus system [24]: working in a TDMA configuration with 7 active beacons, the computed 50% and 90% positioning errors were respectively 2.6 and 4.1 mm. Thus, we have achieved a similar positioning accuracy with a CDMA setup with subtractive compensation of MAI effects than a slower TDMA configuration. Below the 5 mm accuracy level, positioning errors are dominated by other factors than MAI, such as calibration inaccuracy, the effect of finite-size transducers, temperature gradients and air motion through the positioning cell, etc.

#### E. Efficiency of MAI reduction techniques

In this section we will compare the performance of the MAI compensation algorithms to other two possibilities that ameliorate the effects of signal interference in CDMA setups: power control and increased code lengths.

Power control is a technique widely used in wireless communications for interference reduction [17], and consists in adjusting the power of the emitting beacons so that the relative amplitude of their received signals at the mobile beacon is roughly the same. As was mentioned at the end of section III, the present design stage of the 3D-Locus system does not permit to dynamically adjust the beacon signal amplitudes (they can only be set at startup), so power control is only approximately possible in small areas. For trajectory 1 we have measured the received signal amplitudes, one beacon at a time (Fig. 12 (a)), and adjusted the power of each beacon so the received amplitudes are approximately equal (part (b)). Part (c) shows the effect of power control on the MAI outliers. As expected, the total number of outliers before MAI correction is reduced (from 46.4% to 16.4%), and they are approximately equally distributed between all beacons. Application of the simple PIC algorithm achieves a similar performance to power control (16.5% of outliers), while the PIC/ISI algorithm further reduces outliers to 2.2%.

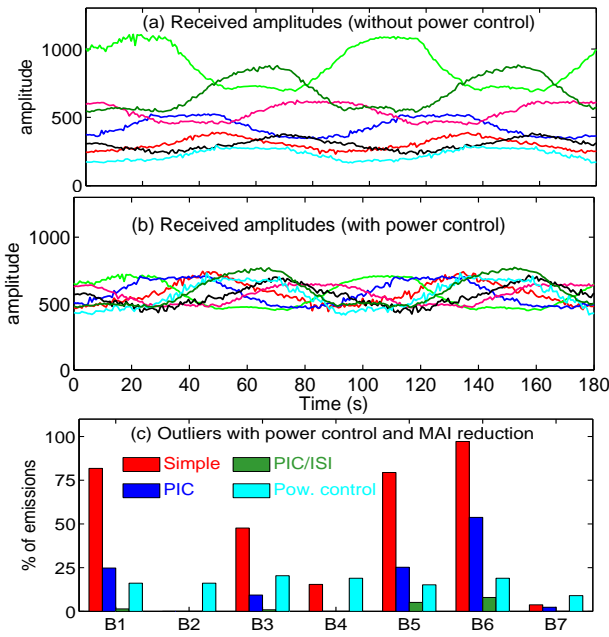


Fig. 12. Comparison of the efficiency for MAI compensation of the PIC and PIC/ISI methods versus power control. Part (a): measured original acoustic amplitudes for trajectory 1 with 7 active beacons; (b) received amplitudes when power control is activated; (c) histogram with the number of outliers obtained in each circumstance.

In conclusion, the simple PIC algorithm has the same effect as employing power control over the emitting beacons, and the PIC/ISI algorithm is superior to power control in terms of outlier reduction.

The other possibility for interference reduction is to increase the code processing gain by using signals with a higher number of bits. To quantify this effect, we repeated trajectory 1 with the 3D-Locus system configured with 32, 64 and 128 bits long signals, and all 7 beacons active. The results are shown in Fig. 13, where we plot the cumulative distribution of the number of valid TOFs per emission (called beacon availability or BA) achieved by each method, as a simple way to compare their relative efficiency for outlier reduction. As expected, augmenting the coded signal's bitlength decreases the number of outliers. However, even with 128 bits long signals, only 10.1% of emissions result in all 7 TOF determined correctly (BA=7). Power control with 32 bits signals is more efficient (26.6% of emissions with BA=7), and performs similarly to MAI compensation with the PIC technique (32.2% of emissions). Finally, the PIC/ISI receiver achieves an 87.4% ratio of emissions with all 7 TOFs free of outliers. Notice that, in addition to increased processing times, the use of spatially longer signals is troublesome due to multipath reflections and, in outer environments, air turbulence or non-uniform propagation which destroy the signal coherence [14].

F. Computational cost of the PIC/ISI algorithm

In practical implementations, MAI compensation techniques should be operative in real-time in the beacon's processing unit. This section gives a brief analysis on the computational cost of the PIC/ISI algorithm described previously.

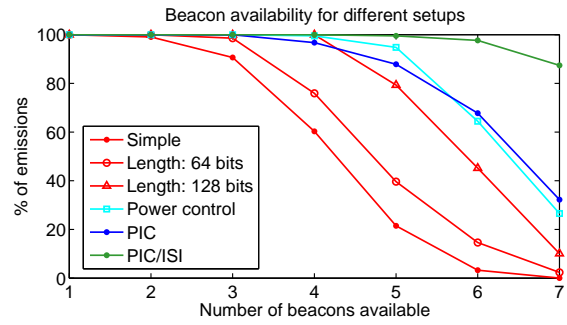


Fig. 13. Comparison of the efficiency in beacon availability of the PIC and the PIC/ISI algorithms with respect to longer signal lengths and use of power control for the transmitting beacon's amplitudes.

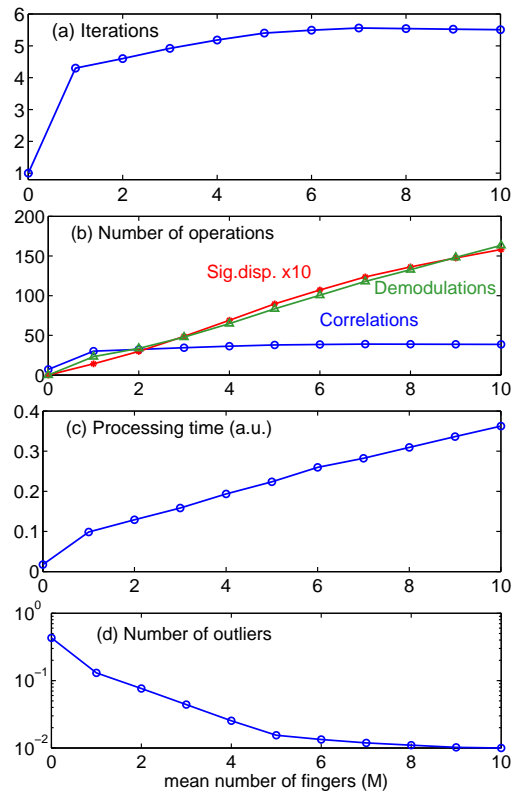


Fig. 14. The computational cost of the PIC/ISI compensation algorithm, for 32 bits signals, and 7 active transmitters: (a) mean number of iterations until convergence; (b) count of the number of three basic operations (per emission); (c) processing time in arbitrary units per emission; (d) fraction of outliers. The abscissa shows the mean number of fingers of the PIC/ISI receiver ( $M = 0$  is the simple receiver and  $M = 1$  the PIC receiver without ISI compensation).

A simple CDMA receiver consists in a correlation bank which requires one set of  $N$  correlations per emission, with  $N$  being the number of active transmitters. Additionally, the PIC algorithm requires signal scaling and displacements, to subtract the estimated transmitter signals, a process which is repeated iteratively until convergence. Finally, the PIC/ISI receiver needs to perform signal demodulations to choose the best candidate TOF. All these aspects have been considered in the experimental evaluation detailed in this section, which corresponds to processing of 32 bits signals, and 7 active transmitters, for trajectories 1 and 2, each repeated three times.

TABLE II  
EFFECTIVENESS OF SUCCESIVE (SIC) AND PARALLEL (PIC)  
INTERFERENCE CANCELATION FOR TWO SAMPLE EXPERIMENTS.

Setup Receiver	TOF outliers (%)				
	Simple	SIC	SIC/ISI	PIC	PIC/ISI
Traj.1; B1-B7, 32 bits	46.5	18.2	10.5	16.5	2.2
Traj.2; B1-B7, 32 bits	40.0	11.3	5.5	9.8	0.9

The averaged results are shown in Fig. 14.

Part (a) of Fig. 14 shows that the number of iterations until convergence of the PIC/ISI algorithm remains relatively constant regardless of the number of fingers employed. The same happens with the number of correlations (part (b)), since only one correlation operation per beacon and iteration is required with the approach of (7). However, the number of signal scaling/displacements and signal demodulations does depend linearly on the number of fingers, as does global computation time (part (c)). Finally, part (d) shows the outlier reduction efficiency respect to the mean number of fingers  $M$ . As seen previously, the PIC/ISI receiver is more efficient than the simple receiver ( $M = 0$  fingers) or the PIC receiver without ISI compensation ( $M = 1$  fingers). Although the fraction of remaining outliers decreases steadily with the number of fingers, in our experimental tests the reduction beyond 5-6 fingers is marginal.

Correlation with the  $g_k$  codes of 3D-Locus is performed efficiently by taking advantage of the properties of Golay codes [25]; for general codes, the Fast Fourier Transform (FFT) can be used. Signal scaling and displacement can be achieved efficiently by time shifting the emitted coded by an integer number of samples ( $\text{round}(t_k/t_s)$ ), and using linear interpolation to adjust for the subsample delay. Finally, demodulation requires signal multiplication of the passband signal with the carrier for conversion to the baseband and a linear-phase FIR filter to eliminate the carrier and integrate and dump the codes [20].

The current processing capability of the microcontroller used for the beacons of the 3D-Locus system does not permit to accommodate the full iterative PIC/ISI algorithm for 7 beacons in the 100 ms emission cycle of the system. Nevertheless, significant reduction of MAI effects is achieved even with one single iteration of the PIC algorithm, as seen in table II. One iteration of the PIC method is equivalent to the Successive Interference Cancellation (SIC) technique frequently used in communication systems [15], in which users are subtracted one at a time in order of descending power. Custom designed acoustic signal processing FPGA architectures, such as those described in [26], [27], as well as more modern DSP processors, could permit operation of the full PIC/ISI algorithm in real time.

## V. CONCLUSIONS

The research carried out on this paper demonstrates that subtractive techniques are very successful in eliminating the range outliers caused by Multiple Access Interference (MAI) in CDMA acoustic positioning systems. We have presented an iterative Parallel Interference Cancellation (PIC) method

TABLE III  
SUMMARY OF ALL EXPERIMENTS REPORTED IN THIS WORK.

Setup Receiver	TOF outliers (%)			Availability (%)		
	Simple	PIC	PIC/ISI	Simple	PIC	PIC/ISI
Traj.1; B2,B3,B4,B7, 32 b.	16.1	0.2	0	42.2	99.1	100
Traj.1; B1,B5,B6,B7, 32 b.	27.3	0.6	0	22.8	97.4	100
Traj.2; B1,B3,B4,B5, 32 b.	31.9	2.2	0.8	18.3	93.0	98.0
Traj.1; B1-B7, 32 bits	46.5	16.5	2.2	60.3	96.7	100
Traj.2; B1-B7, 32 bits	40.0	9.8	0.9	81.2	100	100
Effect of power control (P.C.) and bit length						
Traj.1; B1-B7, 32 b. & P.C.	16.4	3.2	0.4	99.5		
Traj.1; B1-B7, 64 bits	38.4	8.8	0.7	75.9		
Traj.2; B1-B7, 64 bits	29.4	4.4	0.1	93.1		
Traj.1; B1-B7, 128 bits	23.6	2.3	0	100		
Traj.2; B1-B7, 128 bits	19.8	1.2	0.1	100		

which also permits to compensate the effects of intersymbol interference (ISI) due to the acoustic channel limitations.

The effectiveness of MAI compensation has been proved experimentally with as many as 7 beacons functioning simultaneously, and 32 bits long signals. For a low number of transmitting beacons (4), outlier cancellation is nearly complete with either version of the PIC technique. With 7 operating beacons, the simpler version of PIC achieves an outlier reduction by a factor three (from 45% to 15%); if ISI compensation is also applied, outliers are reduced to about 2%.

We have proved that subtractive MAI compensation with 32 bits long signals outperforms using signals of 64 or 128 bits, without the physical inconveniences associated with longer signals (multipath effects, loss of phase coherence and longer acquisition times). Over small displacement areas, we have also shown that the PIC method matches the capability of power control schemes.

The results from the 10 experiments reported in this work are collected in table III; they correspond to about 3500 signal acquisitions under varied setups, most repeated several times. Comparison with the work from other researchers is difficult, since literature on interference cancelation for acoustic positioning systems operating on air is scarce. Only reference [12], in table 2, reports results of Successive Interference Cancellation (SIC) applied to a network of 5 simultaneously emitting piezo transducers, using BPSK modulated signals with 50 kHz carrier frequency and 511 bytes Gold codes. An increase of the availability of the positioning system from 75% to 85% of the events is reported; however, due to the much longer duration of the signals used, MAI effects are not as predominant as in our system.

Finally, an analysis of the number of operations required for the parallel interference cancelation algorithm has been offered, showing that it could be incorporated to modern processing units without introducing excessive overhead. With state of the art acoustic/ultrasonic positioning moving on to CDMA-based system architectures, we believe that MAI compensation techniques should be an essential part of them.

## ACKNOWLEDGMENT

This work was funded by the LORIS project, Spanish Ministry of Economy and Competitiveness (TIN2012-38080-C04-04).

## REFERENCES

- [1] A. Ward, A. Jones, and A. Hopper, "A new location technique for the active office," *IEEE Personal Communications*, vol. 4, no. 5, pp. 42–47, oct 1997.
- [2] N. B. Priyantha, A. Chakraborty, and H. Balakrishnan, "The cricket location-support system," in *Proceedings of the 6th International Conference on Mobile Computing and Networking*, Aug 2000, pp. 32–43.
- [3] J. M. Martín, R. Ceres, L. Calderón *et al.*, "Measuring the 3D-position of a walking vehicle using ultrasonic and electromagnetic waves," *Sensors and Actuators A*, vol. 75, pp. 131–138, 1999.
- [4] F. Figueroa and A. Mahajan, "A robust navigation system for autonomous vehicles using ultrasonics," *Control Engineering Practice*, vol. 2, no. 1, pp. 49–59, February 1994.
- [5] J. Eckert, R. German, and F. Dressler, "An indoor localization framework for four-rotor flying robots using low-power sensor nodes," *IEEE Trans. on Instrumentation and Measurement*, vol. 60, no. 2, pp. 336–344, feb. 2011.
- [6] A. R. Jiménez, J. C. Prieto, J. L. Ealo, J. Guevara, and F. Seco, "A computerized system to determine the provenance of finds in archaeological sites using acoustic signals," *Journal of Archaeological Science*, vol. 36, no. 10, pp. 2415–2426, 2009.
- [7] Y. Ebisawa, "A pilot study on ultrasonic sensor-based measurement of head movement," *IEEE Trans. on Instrumentation and Measurement*, vol. 51, no. 5, pp. 1109–1115, oct 2002.
- [8] H. Kasprzak and D. Iskander, "Ultrasonic measurement of fine head movements in a standard ophthalmic headrest," *IEEE Trans. on Instrumentation and Measurement*, vol. 59, no. 1, pp. 164–170, jan. 2010.
- [9] Hexamite: Ultrasonic industrial positioning systems and ranging. Accessed March 28th, 2014. [Online]. Available: <http://www.hexamite.com/>
- [10] Sonitor: Ultrasound based RTLS for healthcare. Accessed March 28th, 2014. [Online]. Available: <http://www.sonitor.com/>
- [11] J. M. Martín, A. R. Jiménez, F. Seco *et al.*, "Estimating the 3D-position from time delay data of US-waves: experimental analysis and a new processing algorithm," *Sensors and Actuators A*, vol. 101, pp. 311–321, 2002.
- [12] M. Hazas and A. Hopper, "Broadband ultrasonic location systems for improved indoor positioning," *IEEE Trans. on Mobile Computing*, vol. 5, no. 5, pp. 536–547, 2006.
- [13] J. Ureña *et al.*, "Advanced sensorial system for an acoustic LPS," *Microprocessors and Microsystems*, vol. 31, no. 6, pp. 393–401, 2007.
- [14] F. Álvarez, J. Ureña *et al.*, "High reliability outdoor sonar prototype based on efficient signal coding," *IEEE Transactions on Ultrasonics, Ferroelectrics and Frequency Control*, vol. 53, no. 10, pp. 1862–1872, october 2006.
- [15] S. Moshavi, "Multi-user detection for DS-CDMA communications," *IEEE Communications Magazine*, vol. 34, no. 10, pp. 124–136, October 1996.
- [16] A. B. Carlson, *Communication Systems*, 3rd ed. McGraw-Hill, 1986.
- [17] J. Andrews, "Interference cancellation for cellular systems: a contemporary overview," *Wireless Communications, IEEE*, vol. 12, no. 2, pp. 19–29, april 2005.
- [18] M. Stojanovic, "Recent advances in high-speed underwater acoustic communications," *IEEE Journal of Oceanic Engineering*, vol. 21, no. 2, pp. 125–136, 1996.
- [19] I. Céspedes, Y. Huang, J. Ophir, and S. Spratt, "Methods for estimation of subsample time delays of digitized echo signals," *Ultrasonic Imaging*, vol. 17, no. 2, pp. 142–171, 1995.
- [20] J. G. Proakis, *Digital Communications*, 4th ed. McGraw-Hill, 2000.
- [21] D. Divsalar, M. K. Simon, and D. Raphaeli, "Improved parallel interference cancellation for CDMA," *IEEE Trans. on Communications*, vol. 46, no. 2, pp. 258–268, February 1998.
- [22] J. C. Prieto, A. R. Jiménez *et al.*, "Robust regression applied to ultrasound location systems," in *2008 IEEE/ION Symposium on Position, Location and Navigation*, may 2008, pp. 671–678.
- [23] J. C. Prieto, C. Croux, and A. R. Jiménez, "Ropeus: A new robust algorithm for static positioning in ultrasonic systems," *Sensors*, vol. 9, no. 6, pp. 4211–4229, 2009.
- [24] J. C. Prieto, A. R. Jiménez *et al.*, "Performance evaluation of 3D-Locus advanced acoustic LPS," *IEEE Trans. on Instrumentation and Measurement*, vol. 58, no. 8, pp. 2385–2395, aug. 2009.
- [25] B. Popovic, "Efficient Golay correlator," *Electronics Letters*, vol. 35, no. 17, pp. 1427–1428, August 1999.
- [26] A. Hernández *et al.*, "Real-time implementation of an efficient Golay correlator (EGC) applied to ultrasonic sensorial systems," *Microprocessors and Microsystems*, vol. 27, pp. 397–406, 2003.
- [27] A. Suzuki, T. Iyota, and K. Watanabe, *Ultrasonic waves*. Intech, 2012, ch. 9. Real-time distance measurement for indoor positioning system using spread spectrum ultrasonic waves.



**Fernando Seco Granja** was born in 1972 in Madrid, Spain. He holds a B.Sc. degree in Physics (Universidad Complutense de Madrid, 1996) and a PhD in Physics (UNED, 2002), with a dissertation about the magnetostrictive generation of ultrasonic waves applied to a linear position sensor. Since 1997 he has been working at the Center of Automation and Robotics (CAR) of the Consejo Superior de Investigaciones Científicas (CSIC), in Arganda del Rey, Madrid, where he holds a research position. His research interest lies in the design and develop-

ment of indoor Local Positioning Systems (LPS), especially those based on ultrasonic and RF technologies, in signal processing for CDMA systems, and in Bayesian estimation.



**José Carlos Prieto** was born in León, Spain, in 1978. He received the B.Sc. degree in Electronics Engineering from the Universidad de Extremadura, Badajoz, Spain, in 2003, and the Master's degree in robotics from the Universidad Politécnica de Madrid, Spain, in 2007. Since 2004, he has been a Researcher with the Centro de Automática y Robótica, CSIC-UPM, Madrid, and working toward the Doctoral degree in robotics in Universidad de Alcalá. His research interests are focused in ultrasonic localization systems, with special emphasis in signal design and processing, positioning algorithms, robustness, standardization, optimal configurations, calibration methods, and development of new transducers.



**Antonio Ramón Jiménez Ruiz** was born in Santander, Spain, in 1968. He received a B.Sc. degree in physics and computer science and the Ph.D. degree in physics from the Universidad Complutense de Madrid, Spain, in 1991 and 1998, respectively. Since 1993 he has been within the Centro de Automática y Robótica (CAR) that belongs to CSIC (Spanish Council for Scientific Research), Madrid, Spain, where he holds a research position. His research expertise is in the areas of local positioning for indoor/GPS-denied localization and navigation of persons, signal processing, Bayesian estimation and inertial-ultrasonic-RF sensor fusion. He has published over 100 articles in journals and conference proceedings.



**Jorge Guevara** was born in Lima, Peru, in 1978. He received the B.S. degree in electronics engineering from the Universidad Católica Nuestra Señora de la Asunción, Asunción, Paraguay, in 2004. He is currently working toward the Ph.D. degree in electric engineering with the Centro de Automática y Robótica, Consejo Superior de Investigaciones Científicas (CSIC) UPM, Madrid, Spain. His research interests are in the area of localization systems, in particular, automatic calibration methods for ultrasonic positioning